

An X-Band Transformer-Coupled Varactor-Less Quadrature Current-Controlled Oscillator in 0.18 μm SiGe BiCMOS Technology

Xueyang Geng, *Student Member, IEEE*, and Fa Foster Dai, *Fellow, IEEE*

Abstract—This paper presents a transformer-coupled varactor-less quadrature current-controlled oscillator (QCCO) RFIC covering the entire X-Band from 8.7 GHz to 13.8 GHz. The QCCO incorporates a transformer-coupled technique that achieves frequency tuning by varying the bias currents in the primary and secondary windings. Fabricated in a 0.18 μm SiGe BiCMOS technology, the prototype QCCO achieves a 45.3% wide tuning range. With two stacked octagonal transformers the QCCO core circuit occupies $0.4 \times 0.5 \text{ mm}^2$ chip area and draws 8–18 mA current under a 1.8 V power supply. The measured phase noise for 11.02 GHz quadrature outputs is about -110 dBc/Hz at 10 MHz offset. The QCCO achieves a phase noise, power and area efficiency figure-of-merit of -191 dBc/Hz .

Index Terms—Current-controlled oscillator, frequency synthesis, QCCO, quadrature oscillator, SiGe, transformer-coupled oscillator, varactor-less VCO.

I. INTRODUCTION

QUADRATURE signals are widely used in the wireless transceivers as local oscillator (LO) to generate the up- and down-conversions with image-reject mixing. There are several ways to generate quadrature signals. A frequency divider can be used to divide a voltage-controlled oscillator (VCO) output at higher frequency to quadrature phase outputs. The divided-by-four method is usually used because the divided-by-two method requires a 50% duty cycle for the VCO output [1]. However, the divided-by-four method requires a VCO frequency output running at four times the LO frequency, which results in higher power consumption and poor phase noise [2]. The divider method requires the VCO to oscillate at about 40 GHz frequency in order to achieve X-band quadrature outputs. A VCO followed by a passive poly-phase complex filter can be used to generate the quadrature outputs as well [3]. However, the output has poor phase accuracy for wideband operation. In addition, large loss due to the poly-phase network requires power-hungry buffers to boost the LO magnitude. At

higher frequency, a poly-phase filter is very difficult to implement because the reduced component values are more sensitive to process variations and parasitic influences. Cross-coupling two single-phase LC-VCO architectures has been proposed to generate quadrature outputs [4]. This technique provides wideband quadrature accuracy and superior phase noise performance with increased power consumption.

There are various ways to couple the two VCOs and lock their oscillation frequencies. The most commonly used quadrature VCO (QVCO) topology, shown in Fig. 1, utilizes the parallel coupling scheme proposed by Rofougaran *et al.* [5]. The parallel VCO (P-QVCO) delivers quadrature signals with low phase and amplitude errors, yet has a narrow tuning range with the tuning limit of the varactors. In addition, integrated varactors at high frequency such as X-band suffer from poor quality factor, which leads to poor phase noise performance if wide-tuning is needed. Series QVCOs (S-QVCO) have been proposed using CMOS or BiCMOS technology by connecting the coupling transistors in series [6]–[8]. This reduces the noise by using cascode devices and provides better isolation between the VCO output and its current sources. However, the S-QVCO also suffers from a narrow frequency tuning range because of the varactor's narrow tuning capability. A magnetically tuned quadrature oscillator has been reported by Cusmai *et al.*, where the output frequency can be tuned from 3.2 GHz to 7.3 GHz [9] using a 65 nm CMOS technology. Modern communication and radar systems require quadrature signal generation at X- and Ku-bands with wide tuning range for frequency synthesis used in phase-locked loops (PLLs) [10] or direct digital frequency synthesizers (DDSs) [11]–[13]. Most X/Ku-band oscillators are fabricated in InGaP–GaAs technology [14]–[16]. However, InGaP–GaAs technologies have low yield and high power consumption. In addition, they are not compatible with the CMOS and BiCMOS technologies that are widely used for wireless and radar transceiver designs. Although advanced CMOS technologies at 45–65 nm nodes can achieve high operation frequency, the MOSFET suffers from $1/f$ noise and poor Gm efficiency. In the targeted radar transceiver design, SiGe BiCMOS technology is chosen due to its superior noise performance, low power, high current efficiency, and drive capability. As part of the radar transceiver building blocks, an 8.7–13.8 GHz transformer-coupled varactor-less quadrature current-controlled oscillator (QCCO) was implemented in a 0.18 μm SiGe BiCMOS technology [17]. Owing to high cutoff frequency (f_T/f_{max}) of SiGe heterojunction bipolar transistors

Manuscript received January 10, 2010; revised April 13, 2010; accepted May 03, 2010. Date of current version August 25, 2010. This paper was approved by Guest Editor Jean-Baptiste Begueret. This work was supported in part by U.S. Army Research Laboratory and the U.S. Army Space and Missile Defense Command (SMDC) under Contract W911QX-05-C-0003.

The authors are with the Department of Electrical and Computer Engineering, Auburn University, Auburn, AL 36849-5210 USA (e-mail: gengmx@ieee.org; gengxue@auburn.edu; fosterdai@auburn.edu).

Color versions of one or more of the figures in this paper are available online at <http://ieeexplore.ieee.org>.

Digital Object Identifier 10.1109/JSSC.2010.2051266

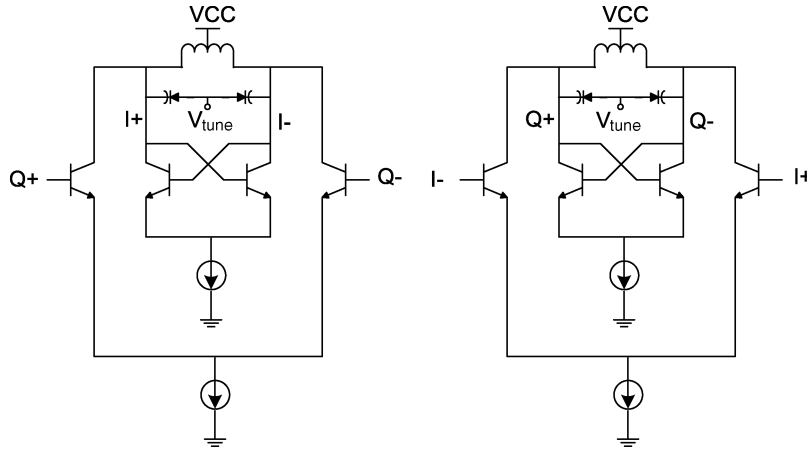


Fig. 1. Quadrature VCO circuits with parallel coupling.

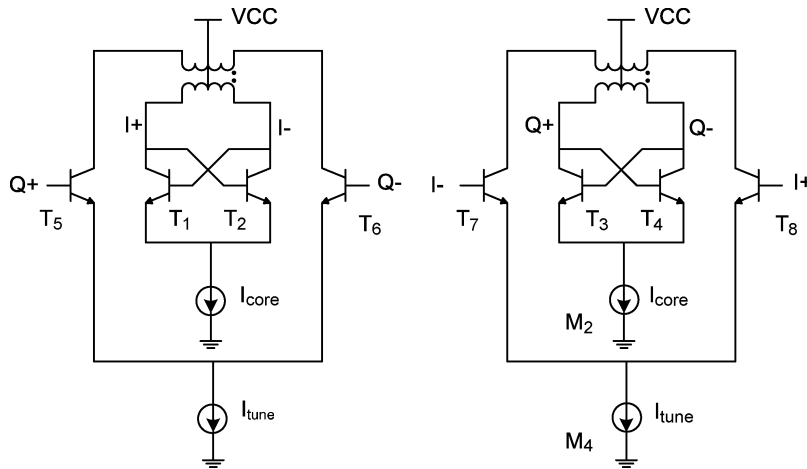


Fig. 2. Schematic of transformer-coupled varactor-less QCCO.

(HBT) and less parasitics compared to its CMOS counterpart, the QCCO presented in this paper was able to achieve quadrature LO generation with wide frequency tuning of 45.3% at X-band frequency, which is highly desirable for radar applications. To our best knowledge, this work represents one of the first X-band quadrature oscillators with transformer-coupled current-controlled tuning mechanism that achieves high oscillation frequency and wide tuning range simultaneously.

This paper is organized as follows. Section II presents the principle and oscillator implementation as well as the phase accuracy and phase noise analysis. Section III discusses the implementation and modeling of the adopted stacked octagonal transformers. Section IV gives the experimental results and the conclusion is given in Section V.

II. ANALYSIS AND DESIGN OF TRANSFORMER COUPLED QUADRATURE OSCILLATOR

A. Oscillation Analysis and Circuit Design

The varactor-less QCCO presented here is a transformer-coupled current-controlled LC oscillator that utilizes SiGe HBT for oscillation and current tuning. For wideband tuning, transformer-coupled technology is employed that achieves

equivalent inductance tuning by varying the bias currents through primary and secondary windings. To achieve the high output frequency, SiGe NPN HBT is used for its small parasitics and low flicker noise. The proposed QCCO circuit is illustrated in Fig. 2, in which two pairs of cross-coupled NPN HBTs, T1, T2 and T3, T4, are used to generate the negative resistances for in-phase CCO (ICCO) and quadrature phase CCO (QCCO) outputs, respectively. Another two pairs of NPN HBTs, T5, T6 and T7, T8, are used to provide the tuning currents for the transformer windings.

Fig. 3 shows an AC equivalent circuit of the ICCO or QCCO circuit. The discussions presented below take ICCO as an example, since the QCCO has the same structure. The primary winding of the transformer has the same function as the LC -tank in the conventional LC coupled oscillators. Negative impedance $-1/g_m$ is generated from the cross-coupled transistor pair T1 and T2. c_p and r_p are the total parasitic resistance and capacitance between the two terminals of the primary transformer winding in the oscillator circuit. The capacitance c_p includes all the transformer parasitic capacitances as well as the transistor parasitic capacitances. The secondary winding is mainly used to tune the effective inductance seen by the tank. Its parasitics, however, are ignorable since they have little impact on

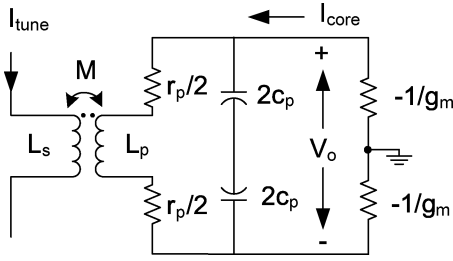


Fig. 3. AC equivalent circuit of the transformer tank.

the QCCO output. To achieve high oscillation frequency, additional capacitors and varactors used in conventional oscillator designs are omitted. With an intuitive analysis based on Fig. 3, the output voltage V_o of the ICCO equivalent circuit can be expressed as

$$\begin{aligned} V_o &= j\omega L_p I_{core} + j\omega M I_{tune} \\ &= j\omega I_{core} (L_p + \alpha M) \end{aligned} \quad (1)$$

where $\alpha = I_{tune}/I_{core}$ is the ratio of the bias currents in the primary (I_{core}) and the secondary (I_{tune}) windings and M is the mutual inductance between the windings. Eq. (1) is used to estimate the equivalent inductance of the oscillation tanks. The parasitic capacitance of the primary winding is treated as the parallel capacitance of the oscillation tanks. The mutual inductance M can be calculated using

$$M = k\sqrt{L_p L_s} \quad (2)$$

where k is the coupling factor of the transformer. Thus, the effective inductance seen by the oscillator tank is given by

$$L_{eff} = L_p + \alpha M. \quad (3)$$

Hence, the oscillation frequency of ICCO and QCCO can be found as

$$f_{osc} = \frac{1}{2\pi\sqrt{(L_p + \alpha M)c_p}}. \quad (4)$$

Note that by varying the tuning current I_{tune} , current ratio α will be altered, which leads to the tuning of the oscillation frequency. Theoretically, α can be tuned arbitrarily by altering the QCCO core current and turning current, and the current flowing direction can be either negative or positive. Thus, the oscillation frequency can be tuned with large tuning range, when α is tuned from a large positive value to a negative value bounded by $-L_p/M$. All the HBTs in the CCO were biased with maximum current near the peak f_T current in order to maximize their switching speed. Although the current tuning will move the bias current off the peak f_T point, great care has been taken to ensure that the f_T frequencies of the devices provide enough switching speed even at their minimum bias currents.

As discussed in the next section, the total parasitic capacitance between the two terminals of the transformer primary winding is only 0.6 pF at 10 GHz frequency. This capacitance does not take into account the device parasitic capacitance.

To achieve the high oscillation frequency, small device parasitic capacitance is desirable. To generate sufficient negative resistance or Gm for sustainable oscillation at high frequency, large current is normally required. If choosing MOSFET as the coupling transistor, large width-to-length (W/L) ratio and large bias current are needed to produce high Gm. In addition, large device size ($W \times L$) is needed to lower the flicker noise of the MOSFET, which unavoidably causes high parasitic capacitance of the devices that further limit the oscillation frequency. On the other hand, HBTs have the following advantages over the MOSFETs that can be utilized to solve the dilemma mentioned above: (i) HBTs have much higher Gm efficiency and require lower current to achieve the same negative impedance; (ii) HBTs have much smaller 1/f noise and thus small device size can be chosen for oscillator design, which further improves the power consumption and oscillation frequency; and (iii) HBTs have less device mismatch, which helps with the quadrature accuracy. Therefore, HBTs at 0.18 μm technology were chosen for the proposed X-band QCCO design.

To determine the actual oscillation frequency, a few more steps on the oscillation conditions need to be derived. According to the circuit analysis for the AC equivalent circuit shown in Fig. 3, the output voltage of the oscillator can be derived as

$$V_o = I_{core} \left[\frac{1}{j\omega c_p} // (r_p + j\omega L_p) \right] - j\omega M I_{tune}. \quad (5)$$

Separating (5) into real and imaginary parts leads to the following expressions for the oscillation amplitude V_o and frequency ω_{osc} :

$$V_o = I_{core} \frac{L_p}{r_p c_p} = I_{core} \cdot \omega_0 Q L_p, \quad (6)$$

$$\begin{aligned} \omega_{osc}^2 &= \omega_0^2 \left[\left(1 - \frac{1}{2m} - \frac{1}{2Q^2} \right) \right. \\ &\quad \left. \pm \frac{1}{2m} \sqrt{\left[\frac{m\omega_0^2}{\omega_c^2} + (3-2m) \right]^2 - 4[(m-1)^2 + 1]} \right] \\ &\approx \omega_0^2 \left[\left(1 - \frac{1}{2m} - \frac{1}{2Q^2} \right) \pm \frac{1}{2m} \sqrt{1-4m} \right] \end{aligned} \quad (7)$$

where $Q = (\omega_0 L_p)/r_p$, $\omega_0 = 1/\sqrt{L_p c_p}$ and $\omega_c = 1/(r_p c_p)$ are the quality factor, self-resonance frequency and corner frequency of the transformer primary winding, respectively. $m = (M/L_p) \cdot (I_{tune}/I_{core})$ can be considered as the coupling strength of the transformer [9], [18], [19]. The oscillation amplitude is independent of the tuning current and is determined only by the core current and the transformer parameters. According to Leeson's equation [20], oscillation amplitude directly affects the output phase noise. Therefore, altering the tuning current in the secondary winding will not affect the phase noise greatly. The approximation of ω_{osc} is acceptable when $\omega_c \gg \omega_0$, which is a valid assumption for the transformer windings. The oscillation frequency is determined by the quality factor of the primary winding as well as m which is a function of the self-inductance and mutual inductance of the

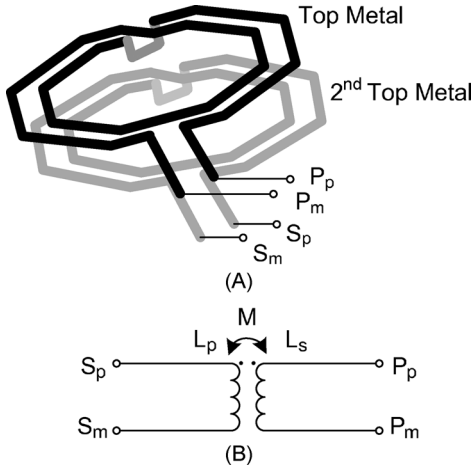


Fig. 4. Stacked octagonal transformer.

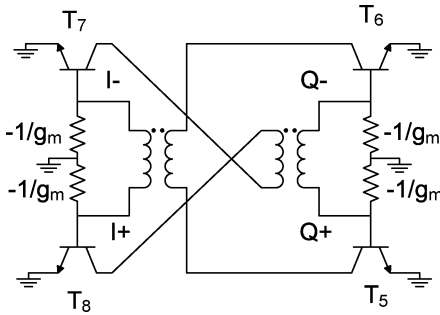


Fig. 5. AC equivalent circuit of the varactor-less QCCO.

transformer and the current ratio of the tuning current to core current. Hence, the proposed tuning scheme by altering the current of the secondary winding provides an efficient means for wideband tuning without degrading the phase noise.

To increase the tuning capability even with small tuning current, the transformer needs to be carefully designed to maximize its coupling efficiency, i.e., its coupling factor or mutual inductance. A stacked octagonal transformer, shown in Fig. 4, which has the maximum mutual inductance compared to other transformer topologies such as concentric and inter-wound, etc., is designed to reduce the magnetic flux leakage [21]. The transformer design is discussed in the following section.

B. Quadrature Phase Accuracy and Phase Noise

Let us evaluate the full AC equivalent circuit of the varactor-less QCCO shown in Fig. 5. If we take T5, T6 and T7, T8 as $-G_m$ amplifiers, Fig. 5 can be further simplified to Fig. 6. Fig. 6(a) shows the transformer in-phase case of the QCCO, while Fig. 6(b) shows the transformer antiphase case of the QCCO. Suppose the phase delay of both $-G_m$ amplifiers is ϕ , based on Barkhausen criteria, the phase delay for the in-phase and antiphase oscillators can be determined by

$$\phi + \phi + \pi = 2n\pi, \quad n = 1, 2, \dots \quad (8)$$

and

$$\phi + \pi + \phi + \pi + \pi = 2n\pi, \quad n = 1, 2, \dots \quad (9)$$

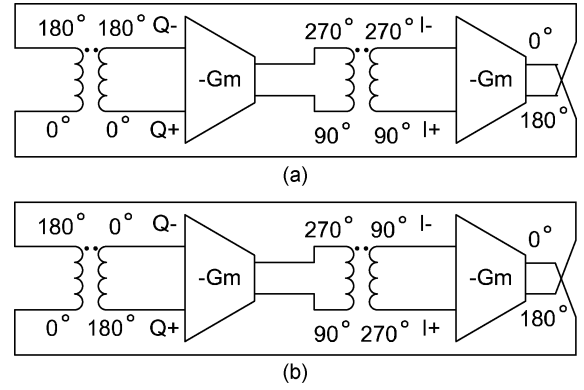


Fig. 6. Equivalent circuits of the varactor-less QCCO. (a) Transformer in-phase. (b) Transformer antiphase.

Thus, the phase delay of the $-G_m$ amplifier is given by

$$\phi = \pm \frac{\pi}{2}. \quad (10)$$

Therefore, regardless of in-phase or antiphase cases, the phase delay between I and Q is always $\pi/2$ or $-\pi/2$. In another word, quadrature frequency outputs can be generated. In practice, there are mismatches between the devices used in the oscillator circuit, which results in slightly different phase delays between the two $-G_m$ amplifiers as well as the two transformers. The device and transformer mismatches are the major contributors of phase error between the quadrature outputs. Another phase error source comes from the coupling between the two transformers used in I oscillator and Q oscillator. From [19], the total phase error ϕ_e can be determined by

$$\phi_e = \frac{1}{2} \frac{Q}{m^2} \varepsilon + k' \frac{Q}{m} \quad (11)$$

where ε represents the mismatches between the devices and transformers, k' is the coupling factor between two primary windings of the transformers that is undesirable in QCCO design, and m is the coupling strength of the transformer defined before. It should be pointed out that the phase error increases with a higher quality factor and a larger transformer coupling strength.

Phase noise of oscillators has been intensively investigated previously [20], [22], [23]. Analysis of the conventional quadrature oscillator has also been presented in [7], [18], [24]. The phase noise of the transformer coupled oscillator is similar to that of the conventional quadrature oscillators discussed in [18], namely,

$$\mathcal{L}(\Delta\omega) = \frac{kt}{C} \cdot \frac{\omega_{osc}}{Q} \cdot \frac{1+m^2}{2} \cdot \frac{1}{\Delta\omega^2} \cdot \frac{1+(1+m)F}{A_0^2} \quad (12)$$

where A_0 is the oscillation amplitude across one of the tanks, and F is the noise factor of the conventional single-phase oscillator. From (12), the phase noise of the quadrature oscillator is degraded rapidly with the increase of m and is reduced with a higher quality factor of coupling inductors or transformers. Hence, a trade-off needs to be considered between the quadrature phase accuracy and oscillator phase noise in order to achieve optimal m and Q in the QCCO design.

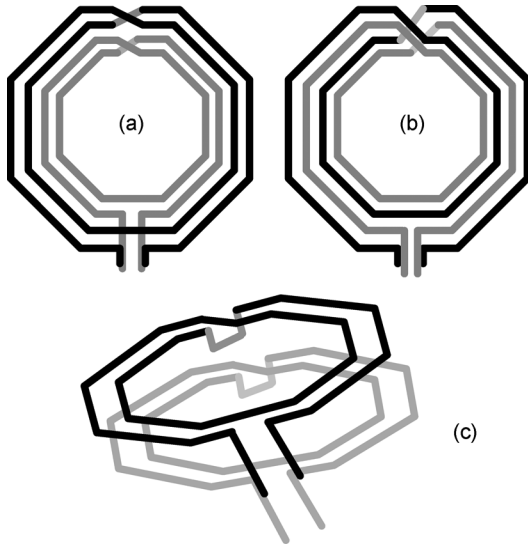


Fig. 7. Octagonal symmetrical transformer: (a) concentric, (b) inter-wound, and (c) stacked.

III. TRANSFORMER IMPLEMENTATION

A. Geometry Design of Transformers

The transformer coupled QCCO has been implemented in a $0.18\ \mu\text{m}$ SiGe BiCMOS technology. The transformer design has been optimized in simulations by means of a full-wave electromagnetic solver, *Agilent Momentum*, in order to maximize magnetic coupling k or the M/L ratio and the primary winding quality factor Q . For different transformer structures, the self-inductance L , the mutual inductance M or the coupling coefficient k , the turn ratio n , the quality factor Q , and the self-resonance frequency ω_0 may vary significantly. Depending on the transformer structures and their magnetic coupling methods (lateral or vertical), different approaches in transformer layout have been proposed [21], [25]. Usually, transformers are formed by magnetically coupling two or more inductors. There are four commonly used inductor shapes: square, hexagonal, octagonal, and circular. Based on these inductors, inter-wound or stacked transformers can be built with different geometrical shapes. Considering the transformer performance (usually inductance and quality factor), the circular shape is the best choice, followed by octagonal and hexagonal structures, and the square inductor is the worst. But the circular layout of the transformers is not compatible with most of the design rules. So the octagonal shape is the most commonly used to build inductors and transformers. For differential circuits, such as what is used in the proposed quadrature oscillator, symmetrical shape is required. Based on the above discussions, Fig. 7 illustrates three transformer topologies: concentric, inter-wound, and stacked. Both the inter-wound and stacked transformers have larger coupling factor than the concentric transformer structure. However, the inter-wound transformer occupies much more area than the stacked one. To trade off the area and coupling factor, the stacked transformer is employed to design the proposed QCCO tank. Fig. 4 shows the adopted stacked transformer drawing diagram with terminal names labeled with respect to the transformer symbol. In this SiGe technology, the top metal layer is much thicker than any

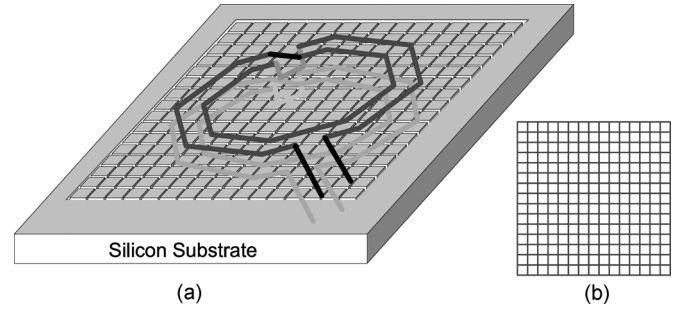


Fig. 8. Diagram of (a) the three-dimensional PGS substrate and (b) the two-dimensional deep trench lattice.

of the other metal layers and stays farthest from the substrate. It is thus used to fabricate the primary winding in order to achieve a good quality factor. While the top metal is thicker than the second-top metal, both top and second-top metals in the chosen $0.18\ \mu\text{m}$ SiGe technology are much thicker than any other metal layers and both are optimized with lower sheet resistance for analog routing. The second-top metal layer, which has the best Q factor compared to any other metal layers except to the top metal, is used to fabricate the secondary windings. Both the primary and secondary windings are $10\ \mu\text{m}$ wide and have two turns with diameter of $200\ \mu\text{m}$. The two windings are exactly overlapped and the winding wire space is $5\ \mu\text{m}$ between the two turns, which is the minimum space allowed by design rules, in order to maximize the fill ratio, defined later. The current maximum rating for the chosen metals is larger than $2.5\ \text{mA}/\mu\text{m}$ for top metal and $0.9\ \text{mA}/\mu\text{m}$ for the second-top metal, which is the worst case scenario assuming all metals stacked on top of each other. Considering the maximum bias current of $5\ \text{mA}$ and the transformer winding dimension of $200\ \mu\text{m}$, the proposed vertically stacked transformer topology will not cause any damage due to localized heating effect.

At low frequencies, the Q of the inductor is limited primarily by the resistance of the metal layer. At high frequency, Q degradation is dominated by the loss mechanisms caused by the substrate [5]. To minimize the Q dependence on the substrate resistivity, the transformer is placed on top of a patterned ground shield (PGS) to minimize the current injected into the substrate. The PGS is a patterned conductive layer and is formed by a lattice of highly resistive deep trench (DT) isolation layer available in the chosen technology. Fig. 8 shows the diagram of the three-dimensional substrate and two-dimensional DT lattice used in this design. The PGS substrate is used to reduce the parasitic capacitance of the transformer to the substrate as well as increase the parasitic resistance to the substrate.

B. Transformer Equivalent Circuit and Parameters

Usually the frequency domain model of the transformer is more important since most performances of the oscillator are analyzed in the frequency domain. However, the time domain equivalent circuit is more intuitive. Fig. 9 shows the $2\text{-}\pi$ equivalent circuit of the stacked transformer. L_p and L_s are the self-inductance of the primary and secondary windings; R_p and R_s are the series resistance of the primary and secondary windings; C_{pp} and C_{ss} are the inter-winding capacitance between the two turns of the primary and secondary winding; and C_{bp} and C_{bs} are the

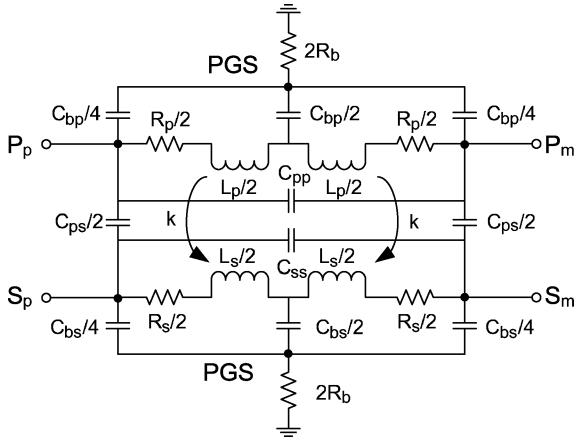


Fig. 9. Transformer time domain equivalent circuit model.

parasitic capacitances of the primary and secondary windings coupled to the PGS, respectively. C_{ps} is the capacitance between the stacked primary and secondary winding, and R_b is the parasitic resistance to the PGS substrate.

The self-inductance for the octagonal inductor can be estimated using Mohan's model [25], namely,

$$L = 2.25 \mu_0 \frac{n^2 d_{avg}}{1 + 3.55\rho} \quad (13)$$

where $d_{avg} = 0.5 (d_{out} + d_{in})$ is the average value of the outer diameter d_{out} and the inner diameter d_{in} of the octagonal inductor. ρ is the fill ratio defined as $\rho = (d_{out} - d_{in}) / (d_{out} + d_{in})$. The mutual inductance M is defined in (2). The coupling factor k of the stacked transformer is more than 0.8.

More accurate self-inductance and mutual inductance or coupling factor can be obtained by electromagnetic simulation and vector network analyzer (VNA) measurement. Fig. 10 shows the simulated parameters of the octagonal stacked transformer. Fig. 10(a) is the plot of primary and secondary self-inductance. They are almost identical since the metal material and thickness does not affect the inductance greatly [21]. Fig. 10(b) shows the coupling factor of the transformer. It is around 0.8 and approaches to 1 at high frequency. Fig. 10(c) is the plot of the quality factor of the primary and secondary windings. The peak Q of the primary winding is about twice of that of the secondary winding because the primary winding metal is thicker and has a lower sheet resistance than the secondary one.

For X-band oscillator design, the parallel capacitance between the terminals of the transformer primary winding is used as the oscillation tank capacitance. The total parallel capacitance is given by

$$C_p = C_{pp} + \frac{C_{bp}}{8} + \frac{C_{ps}}{4} // \left(C_{ss} + \frac{C_{bs}}{8} \right). \quad (14)$$

With the geometry and electronic parameters of the transformer, all these capacitances, C_{pp} , C_{bp} , C_{ps} , C_{ss} , and C_{bs} , can be calculated using the simple parallel-plate capacitor model. The PGS is far away from the windings, so C_{bp} is much smaller than the other capacitances. The accurate frequency dependent capacitance paralleled with the primary winding can be simulated using electromagnetic simulation tools as well. Fig. 11 gives the

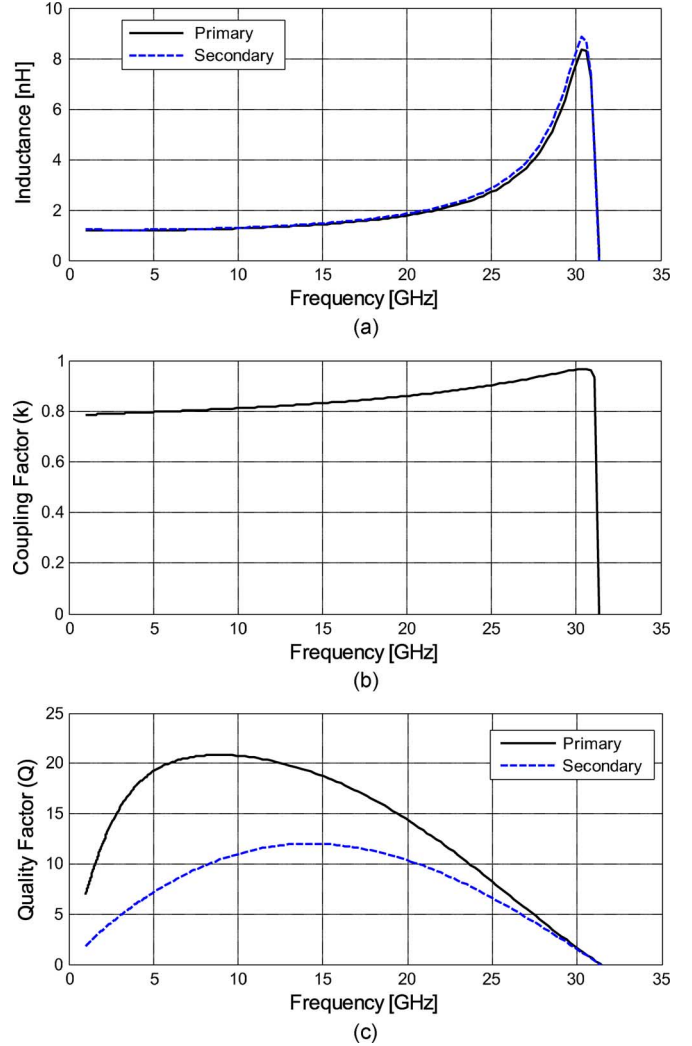


Fig. 10. Simulated parameters of the transformer windings: (a) self-inductance L , (b) coupling factor k , and (c) quality factor Q .

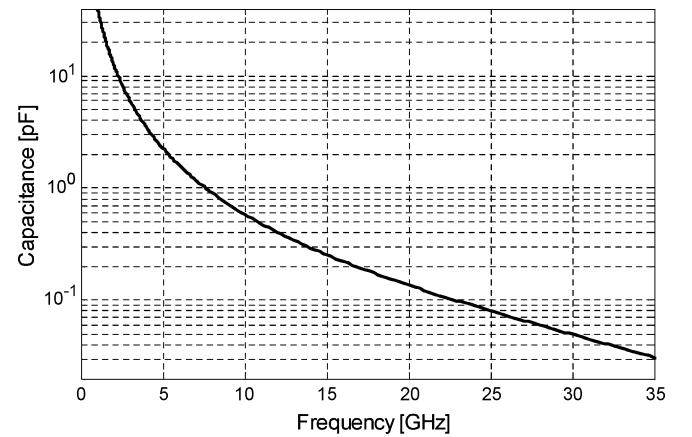


Fig. 11. Simulated capacitance parallel with the transformer primary winding.

plot of the total capacitance with simulated capacitance value of 0.6 pF at 10 GHz frequency.

In practice, it is not easy to find out the exact inductance and capacitance associated with the transformer. With the help of S-parameter simulators, all the simulations can be performed through a hybrid simulation environment. In this design, the

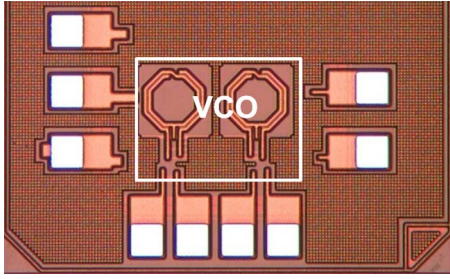


Fig. 12. Fabricated QCCO RFIC die photo.

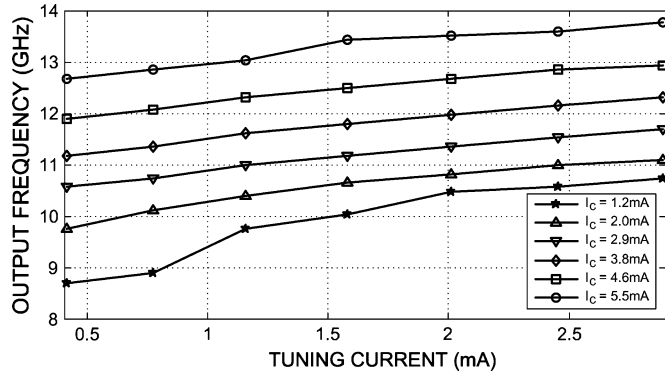


Fig. 13. Measured QCCO tuning range versus tuning current in secondary winding at different core current I_c .

Agilent Dynamic Link tool is used to recall the SPICE simulator and Momentum electromagnetic simulator for all time domain and frequency domain simulations. Therefore, the oscillator was designed by directly specifying the geometric parameters of the transformers instead of giving the L , C parameters in the traditional design flows. The electromagnetic and circuit co-simulation approach adopted here greatly facilitates the transformer design since the time-consuming transformer modeling process is no longer needed.

IV. MEASUREMENT RESULTS

The transformer-coupled varactor-less QCCO was implemented and fabricated in a $0.18 \mu\text{m}$ SiGe BiCMOS technology. The chip die photo is shown in Fig. 12. The QCCO core area is $0.5 \times 0.4 \text{ mm}^2$. As shown in the die photo, the ICCO and QCCO are symmetrically placed. The layout is also optimized to lower the effect of layout parasitic on the QCCO performance including the harmonic distortion and phase noise. The QCCO is tested in CLCC-28 packaged parts. A buffer is included on-chip in order to drive the 50Ω load seen at the input of a spectrum analyzer or a digital oscilloscope. Due to the limitation of the test set-up, all the test results were measured based on the single-ended output, although the QCCO has full differential output capability, which degrades the measured oscillator phase noise and I-Q accuracy.

A wide tuning range of 45.3% is achieved with the tuning current I_{tune} tuned from 0.4 to 2.9 mA and the QCCO core current I_{core} tuned from 1.2 to 5.5 mA. The measured QCCO tuning range is given in Fig. 13. It shows continuous tuning range from 8.7 to 13.8 GHz covering X-band and part of Ku-band. Fig. 14 shows the measured quadrature outputs with 11.5 GHz frequency.

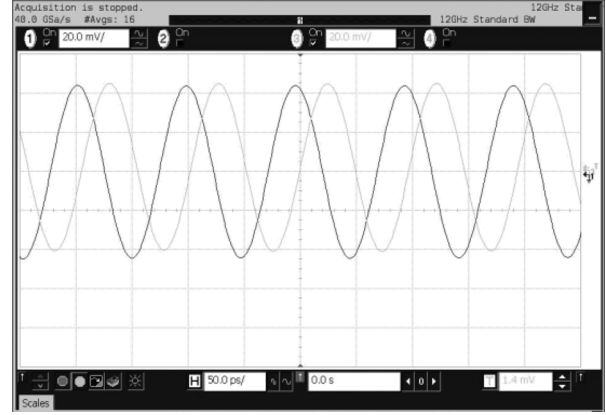


Fig. 14. Measured QCCO outputs at 10.5 GHz with tuning current of 1.5 mA and core current of 2 mA.

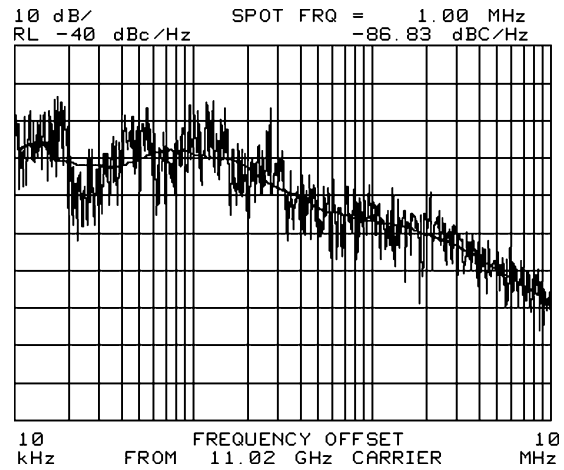


Fig. 15. Measured QCCO phase noise with output frequency of 11.02 GHz.

TABLE I
QCCO PERFORMANCE SUMMARY

| Technology | 0.18 μm SiGe BiCMOS |
|-----------------------|--|
| Supply voltage | 1.8 V |
| Oscillation frequency | 8.7-13.8 GHz |
| Tuning range | 45.3% |
| Core current | 8-18 mA |
| Buffer current | 8 mA |
| Phase noise @ 1MHz | -86.8 dBc/Hz |
| Phase noise @ 10MHz | -110 dBc/Hz |
| QCCO area | $500 \mu\text{m} \times 400 \mu\text{m}$ |
| FOM | -191 dBc/Hz |

The measured phase noise with an 11.02 GHz output frequency is shown in Fig. 15. With the single-ended test, the transformer-coupled varactor-less QCCO achieves -86.8 dBc/Hz phase noise at 1 MHz offset frequency and -110 dBc/Hz at 10 MHz offset frequency. Table I summarizes the measured performances of the transformer-coupled varactor-less QCCO. It achieves 45.3% wide tuning range and the core circuit occupies $0.4 \times 0.5 \text{ mm}^2$ chip area in a $0.18 \mu\text{m}$ SiGe BiCMOS technology. It draws 8–18 mA current over the tuning range under a 1.8 V power supply.

TABLE II
PERFORMANCE COMPARISON OF X/Ku-BAND VARIABLE-FREQUENCY OSCILLATORS

| Ref | Technology | Core Area [mm ²] | Frequency [GHz] | Tuning Percentage | Power [mW] | Phase Noise [dBc/Hz] | FOM [dBc/Hz] | Number of Phases |
|-----------|-----------------------|------------------------------|----------------------------|-------------------|------------|----------------------------|--------------|------------------|
| [14] | InGaP-GaAs HBT | 0.57 | 11.71-12.28 12.71-13.54 | 4.75% 6.3% | 36 48 | -113.8@1MHz -111.8@1MHz | 199 198 | Single phase |
| [15] | InGaP-GaAs HBT | 0.54 | 11.65-12.1 | 3.78% | 25.7 | -108@1MHz | 194 | Single phase |
| [16] | InGaP-GaAs HBT | 1 | 9.46-16.34 | 53.33% | 45 | -90~ -101@1MHz | 188 | Single phase |
| [29] | 90nm CMOS | 0.35 | 10.41-11.37 | 8.8% | 70 | -96.7@1MHz | 194 | 12 polyphases |
| [9]* | 65 nm CMOS | 0.2 | 3.2-7.3 | 67% | 7.2-24 | -120~ -135@1MHz | 229 | Quadrature |
| This Work | 0.18 μ m SiGe HBT | 0.2 | 8.7-13.8 | 45.3% | 14.4-32.4 | -87@1MHz -110@10MHz | 191 204 | Quadrature |

*Note that [9] is listed since it was implemented using a similar architecture.

Several oscillator performance figures-of-merit (FOM) were summarized in [26]–[28], namely,

$$\text{FOM}_A = 10 \log \left(\left(\frac{f_0}{\Delta f} \right)^2 \frac{1 \text{ mW}}{L(\Delta f) \cdot P} \right) \quad (15)$$

$$\text{FOM}_B = 10 \log \left(\left(\frac{f_{\text{tune}}}{\Delta f} \right)^2 \frac{1 \text{ mW}}{L(\Delta f) \cdot P} \right) \quad (16)$$

$$\text{FOM}_C = 10 \log \left(\left(\frac{f_0}{\Delta f} \right)^2 \frac{1 \text{ mW} \cdot 1 \text{ mm}^2}{L(\Delta f) \cdot P \cdot A} \right) \quad (17)$$

where $L(\Delta f)$ is the phase noise at the given offset frequency Δf from the carrier frequency f_0 . Usually, $f_0 = (f_{\text{max}} + f_{\text{min}})/2$ is used to estimate the center oscillation frequency, where f_{max} and f_{min} are defined as the maximum and minimum oscillation frequency. f_{tune} specifies the tuning range of the oscillator, i.e., $f_{\text{tune}} = (f_{\text{max}} - f_{\text{min}})$. P and A are the total core power dissipation and core area of the oscillator. However, FOM_A does not consider the tuning range and area, FOM_B does not include the output frequency, and FOM_C does not account for the tuning range. In this paper, we propose the following FOM to evaluate the oscillator performance considering all important parameters such as phase noise, output frequency, tuning range, power, and area. The revised FOM is given by

$$\begin{aligned} \text{FOM} &= 10 \log \left(\left(\frac{f_0}{\Delta f} \right)^2 \cdot \frac{f_{\text{tune}}}{f_0} \cdot \frac{1 \text{ mW} \cdot 1 \text{ mm}^2}{L(\Delta f) \cdot P_s \cdot A} \right) \\ &= 10 \log \left(\frac{f_0 \cdot f_{\text{tune}}}{\Delta f^2} \cdot \frac{1 \text{ mW} \cdot 1 \text{ mm}^2}{L(\Delta f) \cdot P_s \cdot A} \right) \end{aligned} \quad (18)$$

where P_s is the core power dissipation for the single phase oscillator or equals the total core power divided by the number of phases. The FOM of this transformer-coupled varactor-less QCCO is calculated as -191 dBc/Hz at 1 MHz offset. Table II compares the frequency, tuning range, power consumption, and phase noise for several X/Ku-band oscillators. Although it operates at a lower frequency, the oscillator of [9] is compared

in the table since it was implemented using a similar architecture. Compared to the InGaP-GaAs based oscillators [14]–[16], this QCCO outputs quadrature signals at X-band and has much lower power consumption as well as smaller die area. Compared to the poly-phase oscillator [29], this QCCO has a smaller power consumption, smaller die area and a much higher tuning range.

V. CONCLUSION

A transformer-coupled varactor-less wide tuning QCCO is presented in this paper. It achieves 45.3% wide tuning range by tuning the oscillator currents flowing through the primary and secondary windings of the stacked octagonal transformers. The prototype QCCO is fabricated in 0.18 μ m SiGe BiCMOS technology, and the core circuit occupies 0.4×0.5 mm² chip area with a vertically stacked transformer topology. It draws 8–18 mA current under a 1.8 V power supply. The measured phase noise of the single-ended output is about -86.8 dBc/Hz at 1 MHz offset and -110 dBc/Hz at 10 MHz offset with a 11.02 GHz quadrature outputs. The FOM of this transformer-coupled QCCO is -191 dBc/Hz.

ACKNOWLEDGMENT

The authors would like to acknowledge Geoffrey Goldman at the U.S. Army Research Laboratory and Pete Kirkland at the U.S. Army Space and Missile Defense Command for support.

REFERENCES

- [1] S. L. J. Gierkink, S. Levantino, R. C. Frye, C. Samori, and V. Bocuzzi, "A low-phase-noise 5-GHz CMOS quadrature VCO using superharmonic coupling," *IEEE J. Solid-State Circuits*, vol. 38, no. 7, pp. 1148–1154, Jul. 2003.
- [2] J. W. M. Rogers, F. F. Dai, M. S. Cavin, and D. G. Rahn, "A multi-band $\Delta\Sigma$ fractional-N frequency synthesizer for a MIMO WLAN transceiver RFIC," *IEEE J. Solid-State Circuits*, vol. 40, no. 3, pp. 678–689, Mar. 2005.
- [3] J. Crols and M. Steyaert, "A fully integrated 900 MHz CMOS double quadrature downconverter," in *IEEE Int. Solid-State Circuits Conf. Dig. Tech. Papers*, San Francisco, CA, 1995, pp. 136–137.

- [4] A. Rofougaran *et al.*, "A single-chip 900-MHz spread-spectrum wireless transceiver in 1- μm CMOS. I. Architecture and transmitter design," *IEEE J. Solid-State Circuits*, vol. 33, no. 4, pp. 515–534, Apr. 1998.
- [5] A. Rofougaran, J. Rael, M. Rofougaran, and A. Abidi, "A 900 MHz CMOS LC-oscillator with quadrature outputs," in *IEEE Int. Solid-State Circuits Conf. Dig. Tech. Papers*, 1996, pp. 392–393.
- [6] P. Andreani, A. Bonfanti, L. Romano, and C. Samori, "Analysis and design of a 1.8-GHz CMOS LC quadrature VCO," *IEEE J. Solid-State Circuits*, vol. 37, no. 12, pp. 1737–1747, Dec. 2002.
- [7] P. Andreani and X. Wang, "On the phase-noise and phase error performance of multiphase LC CMOS VCOs," *IEEE J. Solid-State Circuits*, vol. 39, no. 11, pp. 1883–1893, Nov. 2004.
- [8] V. Kakani, F. Dai, and R. C. Jaeger, "A 5-GHz low-power series-coupled BiCMOS quadrature VCO with wide tuning range," *IEEE Microw. Wireless Compon. Lett.*, vol. 17, no. 6, pp. 457–459, Jun. 2007.
- [9] G. Cusmai, M. Repposi, G. Albasini, A. Mazzanti, and F. Svelto, "A magnetically tuned quadrature oscillator," *IEEE J. Solid-State Circuits*, vol. 42, no. 12, pp. 2870–2877, Dec. 2007.
- [10] J. Rogers, C. Plett, and F. Dai, *Integrated Circuit Design for High-Speed Frequency Synthesis*. Boston, MA: Artech House, 2006.
- [11] X. Geng, X. Yu, F. Dai, J. D. Irwin, and R. C. Jaeger, "24-bit 5.0 GHz direct digital synthesizer RFIC with direct digital modulations in 0.13 μm SiGe BiCMOS technology," *IEEE J. Solid-State Circuits*, vol. 45, no. 5, pp. 944–954, May 2010.
- [12] X. Geng, F. F. Dai, J. D. Irwin, and R. C. Jaeger, "An 11-bit 8.6 GHz direct digital synthesizer MMIC with 10-bit segmented sine-weighted DAC," *IEEE J. Solid-State Circuits*, vol. 45, no. 2, pp. 300–313, Feb. 2010.
- [13] X. Yu, F. F. Dai, D. Yang, J. D. Irwin, and R. C. Jaeger, "An X/Ku-band frequency synthesizer using a 9-bit quadrature DDS," in *Proc. IEEE Custom Integrated Circuits Conf. (CICC)*, 2008, pp. 491–494.
- [14] D. Baek, S. Ko, J.-G. Kim, D.-W. Kim, and S. Hong, "Ku-band InGaP-GaAs HBT MMIC VCOs with balanced and differential topologies," *IEEE Trans. Microw. Theory Tech.*, vol. 52, no. 4, pp. 1353–1359, Apr. 2004.
- [15] J. Kim, S. Jeon, S. Moon, N.-Y. Kim, and H. Shin, "A 12-GHz GaInP/GaAs HBT VCO based on push-push output extraction from capacitive common-node," in *IEEE MTT-S Int. Dig.*, 2005, pp. 1705–1708.
- [16] J.-J. Kuo *et al.*, "A wide tuning range voltage controlled oscillator using common-base configuration and inductive feedback," *IEEE Microw. Wireless Compon. Lett.*, vol. 19, no. 10, pp. 653–655, 2009.
- [17] X. Geng and F. F. Dai, "An 8.7–13.8 GHz transformer-coupled varactor-less quadrature current-controlled oscillator," in *Proc. 2009 IEEE Bipolar/BiCMOS Circuits and Technology Meeting (BCTM)*, Capri, Italy, 2009, pp. 63–66.
- [18] L. Romano, S. Levantino, A. Bonfanti, C. Samori, and A. L. Lacaita, "Phase noise and accuracy in quadrature oscillators," in *Proc. IEEE Int. Symp. Circuits and Systems (ISCAS)*, 2006, pp. 161–164.
- [19] A. Mazzanti, F. Svelto, and P. Andreani, "On the amplitude and phase errors of the quadrature LC-tank CMOS oscillators," *IEEE J. Solid-State Circuits*, vol. 41, no. 6, pp. 1305–1313, Jun. 2006.
- [20] D. B. Leeson, "A simple model of feedback oscillator noise spectrum," *Proc. IEEE*, vol. 54, pp. 329–330, Feb. 1966.
- [21] T. H. Lee, *The Design of CMOS Radio-Frequency Integrated Circuits*, 2nd ed. Cambridge, U.K.: Cambridge Univ. Press.
- [22] A. Hajimiri and T. H. Lee, "A general theory of phase noise in electrical oscillators," *IEEE J. Solid-State Circuits*, vol. 33, no. 2, pp. 179–194, Feb. 1998.
- [23] T. H. Lee and A. Hajimiri, "Oscillator phase noise: A tutorial," *IEEE J. Solid-State Circuits*, vol. 35, no. 3, pp. 326–336, Mar. 2000.
- [24] A. Andreani, "A time-variant analysis of the $1/f^2$ phase noise in CMOS parallel LC-tank quadrature oscillators," *IEEE Trans. Circuits Syst. I*, vol. 53, no. 8, pp. 1749–1770, Aug. 2006.
- [25] S. S. Mohan, M. D. Hershenson, S. P. Boyd, and T. H. Lee, "Simple accurate expressions for planar spiral inductances," *IEEE J. Solid-State Circuits*, vol. 34, no. 10, pp. 1419–1424, Oct. 1999.
- [26] P. Kinget, "Integrated GHz voltage controlled oscillators," in *Analog Circuit Design: (X)DSL and Other Communication Systems; RF MOST Models; Integrated Filters and Oscillators*. Boston, MA: Kluwer Academic, 1999, pp. 353–381.
- [27] P. Kinget, B. Soltanian, S. Xu, S. Yu, and F. Zhang, "Advanced design techniques for integrated voltage controlled LC oscillators," in *Proc. 2007 IEEE Custom Integrated Circuits Conf. (CICC)*, 2007, pp. 805–811.
- [28] D. Ham and A. Hajimiri, "Concepts and methods in optimization of integrated LC VCOs," *IEEE J. Solid-State Circuits*, vol. 36, no. 6, pp. 896–909, Jun. 2001.
- [29] N. Tzartzanis and W. W. Walker, "A reversible poly-phase distributed VCO," in *IEEE Int. Solid-State Circuits Conf. Dig. Tech. Papers*, San Francisco, CA, 2006.



Xueyang Geng (S'08) received the Ph.D. degree in electrical and computer engineering from Auburn University, Auburn, AL, in 2010, the M.S. degree from the Institute of Semiconductors, Chinese Academy of Sciences, Beijing, China, in 2004, and the B.S. degree in physics from the University of Science and Technology of China (USTC), Hefei, China, in 2001.

From 2004 to 2005, he was with STMicroelectronics Design Center, Shenzhen, China, where he was working on high-voltage power regulator ASIC design in BCD technology. His research interests include VLSI circuits for mixed-signal, analog and RF applications, oscillators, phase-locked loops, ultrahigh-speed direct digital synthesis (DDS), and digital-to-analog converters.



Fa Foster Dai (M'92–SM'00–F'09) received the Ph.D. degree in electrical and computer engineering from Auburn University, Auburn, AL, in 1997 and the Ph.D. degree in electrical engineering from The Pennsylvania State University, University Park, PA, in 1998.

From 1997 to 2000, he was with Hughes Network Systems of Hughes Electronics, Germantown, MD, where he was a Member of Technical Staff in very large scale integration (VLSI), designing analog and digital ICs for wireless and satellite communications. From 2000 to 2001, he was with YAFO Networks, Hanover, MD, where he was a Technical Manager and a Principal Engineer in VLSI designs, leading high-speed SiGe IC designs for fiber communications. From 2001 to 2002, he was with Cognio Inc., Gaithersburg, MD, designing radio frequency (RF) ICs for integrated multi-band MIMO wireless transceivers. From 2002 to 2004, he was an RFIC consultant for Cognio Inc. In August 2002, he joined Auburn University in Auburn, AL, where he is currently a Professor in electrical and computer engineering. His research interests include VLSI circuits for analog and mixed-signal applications, RFIC designs for wireless and broadband networks, ultrahigh frequency synthesis and mixed signal built-in self-test (BIST). He co-authored the book *Integrated Circuit Design for High-Speed Frequency Synthesis* (Artech House, 2006).

Dr. Dai has served as Guest Editor for IEEE TRANSACTIONS ON INDUSTRIAL ELECTRONICS in 2001, 2009, and 2010. He served on the technical program committee of the IEEE Symposium on VLSI Circuits from 2005 to 2008. He currently serves on the technical program committee of the IEEE Custom Integrated Circuits Conference (CICC), and the IEEE Bipolar/BiCMOS Circuits and Technology Meeting (BCTM). He holds five U.S. patents and received the Senior Faculty Research Award for Excellence from the College of Engineering of Auburn University in 2009.